Mon. Not. R. Astron. Soc. **000**, 000–000 (0000) Printed 28 January 2016 (MN LATEX style file v2.2)

# Galaxy Zoo: Morphological Classifications for Galaxies in HST Legacy Imaging

Lead Author and other Galaxy Zoo science team members

*This publication has been made possible by the participation of more than 200,000 volunteers in the Galaxy Zoo project. Their contributions are individually acknowledged at http://authors.galaxyzoo.org/authors.html.

E-mail: lead.author@university.edu

28 January 2016

**ABSTRACT**

This will be the data release paper for GZ Hubble. We present the classifications, the methodology for data reduction and corrections for redshift dependent biases in the observed morphologies.

## 1 INTRODUCTION

## 2 SAMPLE AND DATA

### 2.1 Summary of HST Legacy Survey Imaging

- AEGIS has 1 orbit each ($\sim$ 2200 seconds) in the F606W (V-band) and F814W (I-band) filters and has been dithered to 0.03 ″/pixel; the imaging covers $\sim$ 710 arcmin$^2$.
- GOODS targeted 2 fields, GOODS-N and GOODS-S, imaging in 4 filters – F435W (B), F606W (V), F775W (i), and F850LP (z). The mean exposure times vary, from 1000 – 2100 seconds. The images have been dithered to a pixel scale of 0.03 ″/pixel and covers a total area of $\sim$ 320 arcmin$^2$ (160 arcmin$^2$ per field). The filters that Griffith et al. (2012) uses for the colored images were F606W and F775W for GOODS-N and F606W and F850LP for GOODS-S.
- COSMOS has 1 orbit (2028 seconds) in the F814W (I-band) filter and has been dithered to 0.05 ″/pixel; it covers the largest area, $\sim$ 1.8 deg$^2$.
- GEMS has 1 orbit (2160 and 2286 seconds in the F606W and F850LP filters, respectively) with a pixel scale of 0.03 ″/pixel; it covers $\sim$ 800 arcmin$^2$

### 2.2 User weighting

The votes of individual users who classified galaxies in Galaxy Zoo Hubble are combined to make a vote fraction for each question on the classification tree. Users votes are weighted slightly (in a method identical to that described in Willett et al. 2013) such that users who frequently disagree with all other users end up having very low weights. The majority of users have weights very close to 1.0 (**STEVEN: Is this true for GZH - do you have a plot of the distribution of user weights or consistencies we can include here?**.

## 3 CORRECTING FOR REDSHIFT-DEPENDENT CLASSIFICATION BIAS

Previous version of Galaxy Zoo morphology classifications (Lintott et al. 2008; Willett et al. 2013) were based on observations of galaxies in the Sloan Digital Sky Survey (SDSS) which are typically at $z < 0.1$. In these cases it could be assumed that there was no real evolution of the morphologies of galaxies and therefore any observed changes in the distribution of galaxies with different consensus morphologies was assumed to be due to the effects of redshift on the image quality (*i.e.*. the reduction in physical resolution, surface brightness dimming etc). So for both previous releases of GZ morphogloies, a correction was provided for redshift dependent bias based on matching the classification fractions at the highest redshfts with those at the lowest redshift. See Bamford et al. (2009) and Willett et al. (2013) for the details.

In the GZH samples the redshift range is so large that we expect to find redshift evolution of the types and morphologies of galaxies which are seen. So the previous methods of correcting for redshift dependent bias will not work. In addition the effects of band shifting will change the images even more across these redshift ranges.

In order to test the effects of redshift we made images of the same galaxy at a variety of redshifts using input images from the SDSS (York et al. 2000; Strauss et al. 2002) and the FERENGI code (Barden et al. 2008) to produce images that match the observational properties of those observed in the HST surveys. These images were classified in the Galaxy Zoo interface using the same classification scheme as the original HST images.

### 3.1 Selection of FERENGI Input Galaxies

We selected 288 unique galaxies from SDSS imaging to run through the FERENGI code. The selection spanned a variety

**Table 1.** Summary of Galaxy Zoo: Hubble imaging

| Survey | $t_{\rm exp}$ [sec] | Filters | Resolution [″/pix] | Area [arcmin$^2$] | $N_{\rm galaxies}$ |
|---|---|---|---|---|---|
| AEGIS | 2200 | F606W (V) and F814W (I) | 0.03 | 710 | 8157 |
| COSMOS | 2028 | F814W (I) | 0.05 | 6480 | 88530 |
| GEMS | 2160−2286 | F606W (V) and F850LP (z) | 0.03 | 800 | 9143 |
| GOODS | 1000−2100 | F435W (B), F606W (V), F775W (i), F850LP (z) | 0.03 | 320 | 7336 |
| *GOODS-N* | – | – | – | – | *2551* |
| *GOODS-S* | – | – | – | – | *4785* |
| total | – | – | – | 8310 | 113166 |

**Table 3.** Summary of FERENGI artificial redshifting

| $z_{\rm target}$ | $N_{z\rm bins}$ | $N_{\rm evolution}$ | $e_{\rm max}$ | $N_{\rm galaxies}$ | $N_{\rm images}$ |
|---|---|---|---|---|---|
| 0.3 | 8 | 7 | −3.0 | 72 | 4032 |
| 0.5 | 6 | 4 | −1.5 | 72 | 1728 |
| 0.8 | 3 | 3 | −1.0 | 72 | 648 |
| 1.0 | 1 | 3 | −1.0 | 72 | 216 |

of galaxy morphologies (as selected by GZ2 classifications) and $r'$-band surface brightnesses, and also spanned the redshift range of SDSS targets (in $N_z = 4$ bins) in order to be optimised for different target minimum redshifts in HST imaging.

The selection criteria for the different morphological categories is summarised in Table 2. The surface brightness selection ($N_\mu = 3$) was (1) low: $\mu > 21.5$ mag arcsec$^{-2}$; (2) mid: $20.5 < \mu < 21.5$ mag arcsec$^{-2}$; and (3) high: $\mu < 20.5$ mag arcsec$^{-2}$. For each of the four "target redshifts" ($z = 0.3, 0.5, 0.8$ and 1.0), the images were redshifted in $\Delta z = 0.1$ bins up to $z = 1.0$.

In addition to the physical parameters of the input images, the FERENGI output depends on assumptions of the global galaxy evolution model. This evolution is a crude mechanism that mimics the brightness increase of galaxies with increasing redshift (out to at least $z \sim 1-2$). The effect on the redshifted images is simply an empirical addition to the magnitude of a galaxy of the form $M' = e \times z + M$, where $M'$ is the corrected magnitude, and $e$ is the evolutionary correction in magnitudes (i.e., $e = -1$ essentially brightens the galaxy by 1 magnitude by $z = 1$). We ran FERENGI for values of $e$ starting from $e = 0$ and decreasing to $e = -3.5$ in increments of $\Delta e = 0.5$. Figure 1 shows several examples of the effects of "losing" spiral/disc features with increasing redshift for two galaxies with $e = 0$.

The final number of FERENGI images produced for each galaxy is a ultimately a function of galaxy's redshift, since the code cannot resample the images at better angular resolution than the original SDSS data, and the number of $e$ values selected. Table 3 summarizes the total sample of redshifted images produced for GZ: Hubble.

### 3.2 Correcting GZH morphologies for classification bias

The approach used in GZH for correcting the weighted classifications for user bias rests on the assumption that the *amount* of bias is a function of the apparent size and brightness of the image as seen on screen. This is controlled by two types of parameters: **intrinsic** properties of the galaxy itself, such as its physical diameter and luminosity, and **extrinsic** properties, such as the distance (redshift) of the galaxy and its relative orientation. There are likely other parameters that affect user accuracy, such as the proximity of close companions ("distraction bias"; see Johnson et al. 2015) or those that vary by individual user. The combination of all such parameters forms a high-dimensional space, and we have insufficient test galaxies to measure the individual effects of each. Instead, we use just two parameters that are intended to capture the bulk of the change in bias (based on GZ1/GZ2): a galaxy's $r'$-band surface brightness ($\mu_r$; intrinsic) and redshift ($z$; extrinsic).

The change in bias as a function of $\mu_r$ and $z$ is measured using the FERENGI images over all the evolutionary corrected factors. We assume that the "true" (ie, debiased) vote fraction $f_{\mu,z}$ for a galaxy can be expressed as:

$$f_{\mu,z} = (f_{\mu,z=0.3}) \times e^{\frac{z-z_0}{\zeta}}, \quad (1)$$

where $f_{\mu,z=0.3}$ is the "calibrated" vote fraction at the lowest redshift in the FERENGI bins, which is at redshift $z = 0.3$ and $\zeta$ is a positive parameter that controls the rate at which $f$ drops off with increasing redshift. This formula fits the data relatively well (with almost no exceptions, the vote fractions for featured galaxies decrease monotonically with increasing redshift), and the exponential function bounds the observed vote fractions between $f_{\mu,z=0.3}$ and zero. Figure 2 show examples of the change in vote fraction and their fits to Equation 1 for a random selection of galaxies in the FERENGI images.

We then take the values of $\zeta$ for *all* sets of artifically redshifted galaxies and use them to fit the overall distribution of $\zeta$ as a function of surface brightness (since we expect the correction being applied to vary as a function of the intrinsic galaxy properties). We restrict the galaxies that can be used to measure the calibration to those with data at the pivot redshift of $z = 0.3$, those with non-zero $f_{\rm features}$ at $z = 0.3$, and with a reasonable fit to the exponential model ($\Delta\chi^2 > 3.0$).

Figure 3 shows the results of the sample; the correction is a weak function of surface brightness overall. Higher-surface brightness galaxies have stronger average corrections, likely because these galaxies are more likely to have larger $f_{\rm features}$ values at high redshifts. Low surface brightness galaxies are more likely to begin low and remain low;

**Table 2.** Summary of morphological categories selected for FERENGI sample. For Edmond: does $p_{\rm obvious/dominant} > 0.5$ mean ($p_{\rm obv} + p_{\rm dom} > 0.5$) or ($p_{\rm ob}$ OR $p_{\rm dom} > 0.5$)?

| Morphology | Label | Selection | $N_{\rm objects}$ $[N_z \times N_\mu]$ |
|---|---|---|---|
| Features | Yes | $p_{\rm features} > 0.8$, $p_{\rm odd} < 0.1$ | 12 |
| | Int | $0.3 < p_{\rm smooth} < 0.6$, $p_{\rm odd} < 0.1$ | 12 |
| | No | $p_{\rm smooth} > 0.8$, $p_{\rm odd} < 0.1$ | 12 |
| Merger | No | $p_{\rm features} > 0.8$, $p_{\rm odd<0.1}$, $p_{\rm merger} < 0.1$ | 12 |
| | Int | $p_{\rm odd} > 0.5$, $0.1 < p_{\rm merger} < 0.4$ | 12 |
| | Yes | $p_{\rm odd} > 0.5$, $p_{\rm merger} > 0.4$ | 12 |
| Edge-on | Yes | $p_{\rm edgeon} > 0.8$, $p_{\rm features} > 0.5$ | 12 |
| | Int | $0.4 < p_{\rm edgeon} < 0.8$ , $p_{\rm features} > 0.5$ | 12 |
| | No | $p_{\rm edgeon} < 0.2$, $p_{\rm features} > 0.5$ | 12 |
| Bar | No | $p_{\rm bar} < 0.1$, $p_{\rm features} > 0.5$, $p_{\rm edgeon} < 0.2$ | 24 |
| | Int | $0.2 < p_{\rm bar} < 0.4$, $p_{\rm features} > 0.5$, $p_{\rm edgeon} < 0.2$ | 24 |
| | Yes | $p_{\rm bar} > 0.8$, $p_{\rm features} > 0.5$, $p_{\rm edgeon} < 0.2$ | 24 |
| Visible spiral | No | $p_{\rm spiral} < 0.2$, $p_{\rm features} > 0.5$, $p_{\rm edgeon} < 0.2$, $p_{\rm bar} < 0.1$ | 12 |
| | Int | $0.2 < p_{\rm spiral} < 0.8$, $p_{\rm features} > 0.5$, $p_{\rm edgeon} < 0.2$, $p_{\rm bar} < 0.1$ | 12 |
| | Yes | $p_{\rm spiral} > 0.8$, $p_{\rm features} > 0.5$, $p_{\rm edgeon} < 0.2$, $p_{\rm bar} < 0.1$ | 12 |
| Oblique bulge size | No | $p_{\rm nobulge>0.6}$, $p_{\rm features} > 0.5$, $p_{\rm edgeon} < 0.5$, $p_{\rm bar} < 0.2$ | 12 |
| | Int | $p_{\rm justnoticeable} > 0.6$, $p_{\rm features} > 0.5$, $p_{\rm edgeon} < 0.5$, $p_{\rm bar} < 0.2$ | 12 |
| | Yes | $p_{\rm obvious/dominant} > 0.5$, $p_{\rm features} > 0.5$, $p_{\rm edgeon} < 0.5$, $p_{\rm bar} < 0.2$ | 12 |
| Edge-on bulge shape | Round | $p_{\rm rounded} > 0.5$, $p_{\rm features} > 0.5$, $p_{\rm edgeon} > 0.5$ | 12 |
| | Boxy | $p_{\rm boxy} > 0.4$, $p_{\rm features} > 0.5$, $p_{\rm edgeon} > 0.2$ | 12 |
| | Non | $p_{\rm nobulge} > 0.5$, $p_{\rm features} > 0.5$, $p_{\rm edgeon} > 0.5$ | 12 |

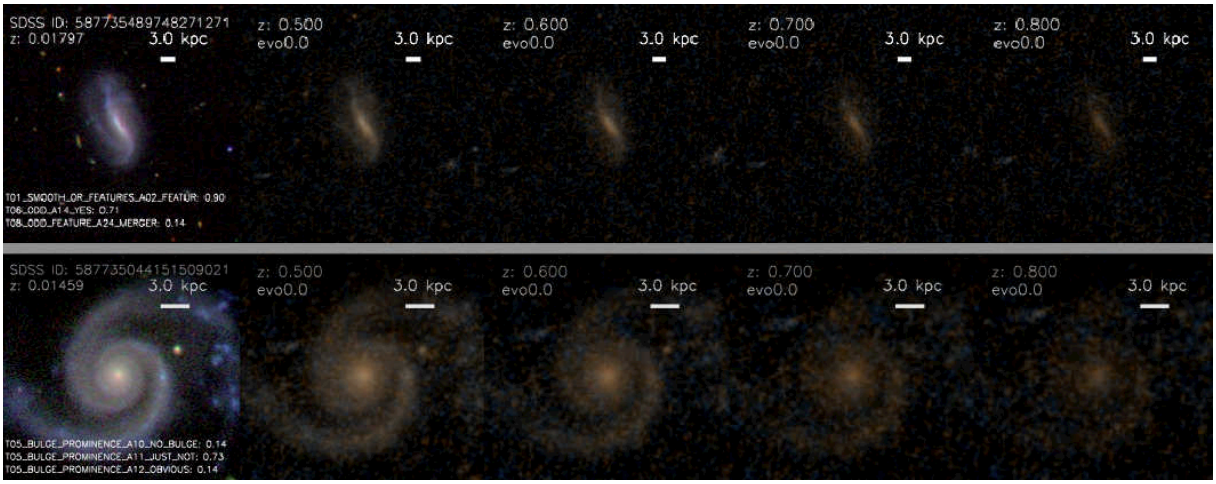


**Figure 1.** Examples of two galaxies which have been run through the FERENGI code to produce simulated HST images. The value of $p_{\rm features}$ for each panel is (1) Top row: $p_{\rm features} = 0.9, 0.625, 0.35, 0.35, 0.225$ and (2) Bottom row: $p_{\rm features} = 1.00, 0.875, 0.875, 0.625, 0.375$.

the bounded nature of the dropoff (and Poissonian-like variance among the individual voters) means that the average magnitude of $\zeta$ will be less.

We fit the data in Figure 3 with a linear function such that:

$$\log_{10}(\hat{\zeta}) = \zeta_0 + \zeta_1 \times \mu, \quad (2)$$

where $\hat{\zeta}$ is the correction factor that will be applied to each galaxy as a function of surface brightness. The best-fit parameters to the linear fit (from least-squares optimization) are $\zeta_0 = 0.1, \zeta_1 = 1.4$. To make the final debiased correction, we modify the simple exponential form of Equation 1 to bound the debiased vote fractions between $f$ and 1:

$$f_{\rm debiased} = 1 - (1 - f)e^{\frac{z - z_0}{\zeta}}. \quad (3)$$

### 3.3 Results of $\zeta$ approach

In Figure 5 we examine the change in $p_{\rm features}$ for the FERENGI galaxies relative to their lowest simulated redshift. In this analysis, only galaxies whose lowest simulated redshift image was ($z_{\rm sim} = 0.3$) were used (see Table 3), and only those which had detectable surface brightness measurements in Sextractor; this includes 3,959 of the total 6,466 images. For each simulated redshift value $z$, and at fixed surface brightness $\mu$, we plot $p_{\rm features,z}$, the value measured at that

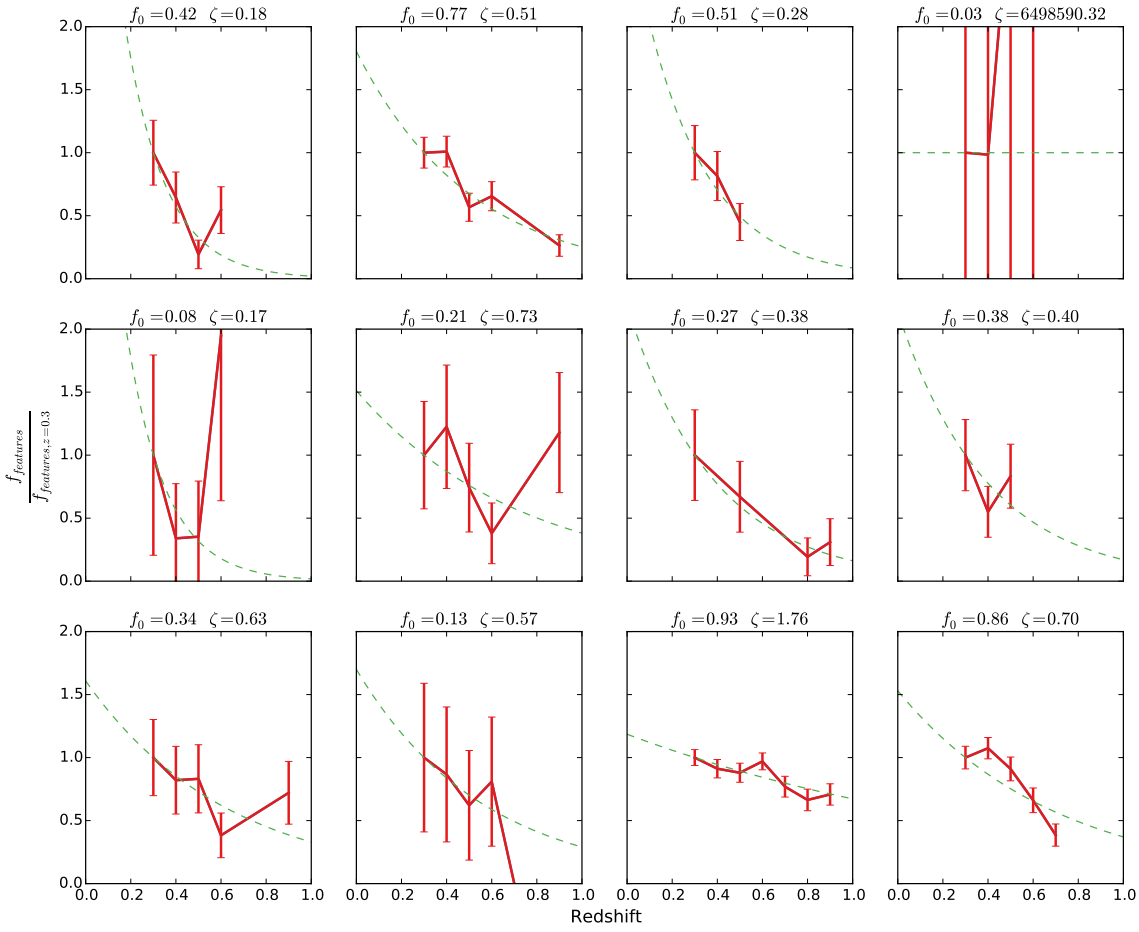


**Figure 2.** Behavior of the normalized, weighted vote fractions of features visible in a galaxy ($f_{\rm features}$) as a function of redshift in the artifical FERENGI images. Galaxies are a random selection of images with $e = 0$ and at least three detectable images in redshift bins of $z \geq 0.3$. The measured vote fractions (red points) are fit with an exponential function (Equation 1); the best-fit parameters are given above each plot. Error bars are Poissonian, assuming a median of 40 votes per galaxy.

simulated redshift, vs $p_{\rm features,z=0.3}$, the value measured for the same galaxy imaged at $z = 0.3$.

Our objective is to use these data to predict, for a galaxy with a measured $p_{\rm features,z}$ value, what its $p_{\rm features}$ value would have been if it had been viewed at $z = 0.3$. This predicted value is defined as the debiased vote fraction $p_{\rm features,debiased}$, and is calculated by applying a correction to the measured value of $p_{\rm features}$, determined by the $\zeta$ function described in the previous section. We determine that a predicted value can be obtained so long as the relationship between $p_{\rm features,z}$ and $p_{\rm features,z=0.3}$ is single-valued; that is, for a given $p_{\rm features,z}$, there is one corresponding value of $p_{\rm features}$ at $z = 0.3$.

In Figure 5 we see that the relationship between $p_{\rm features,z}$ and $p_{\rm features,z=0.3}$ is *not* always single valued; hence we do not find it appropriate to correct galaxies that lie in these regions of surface brightness/redshift/$p_{\rm features}$ space. These regions tend to have low $p_{\rm features}$ values at high redshift, but a wide range of values at $z = 0.3$. These regions contain two morphological types of galaxies: First are genuine ellipticals, which have low values of $p_{\rm features}$ at both high and low redshift. Second are disks whose features become washed out at high redshift; hence their $p_{\rm freatures}$ value at $z = 0.3$ may be quite high, while the value observed at high redshift is very low. This effect is strongest at the highest redshift and the lowest surface brightnesses, where features become near impossible to discern from the images. From this information we conclude that, for the Hubble galaxies, we cannot distinguish between genuine ellipticals and disks if the measured value of $p_{\rm features}$ is too low for a given surface brightness and redshift, because the relationship between the measured value and the "original" ($z = 0.3$) value is not single-valued.

Our criteria for determining whether a region of this space is single-valued, and therefore correctable, is as follows: For each surface brightness and redshift bin, we exam-

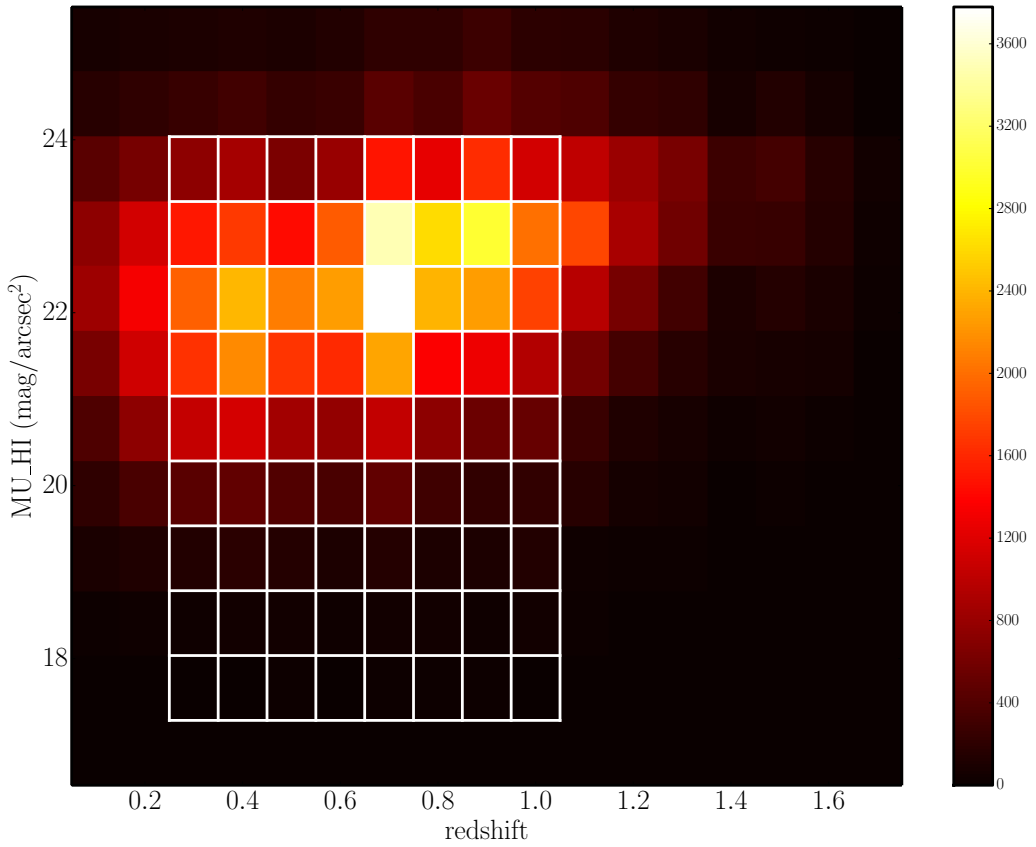


**Figure 4.** Surface brightness vs. redshift of 118,083 galaxies in the ACS Hubble sample. The white grid denotes the surface brightness and redshift range of the FERENGI images, subdivided in bins corresponding to fixed ranges used for analysis in Figure 5.

ine the distribution of $p_{\mathrm{features,z=0.3}}$ in four bins of $p_{\mathrm{features,z}}$. These sub-bins are marked by the horizontal lines within each larger, surface brightness/redshift bin in Figure 5. First, we compute the interquartile range (IQR) of the distribution of $p_{\mathrm{features,z=0.3}}$ in each sub-bin, which are indicated by the orange bars. For the region to be considered correctable, we require that the IQR of the distribution within these sub-bins is less than the sub-bin height. Regions which fit these criteria are uncouloured in the plot. If the IQR is greater than the bin height, the region is considered uncorrectable; these are marked in green. Any region with fewer than 5 points is considered to have "not enough information (NEI)", and are shown in purple.

Using this approach, 52% of the FERENGI images were found to have single-valued relationships between their $p_{\mathrm{features}}$ values at high and low redshift (see Table 4 for a summary.) Only these images were used in determining the $\zeta$ function (Section 3.2).

Stuff to do in this section:

- talk about where the Hubble sample falls in this space, reference table 5

**Table 4.** Distribution of FERENGI images analysed in Figure 5. Correctable images had a single-valued relationship between their measured $p_{\mathrm{features}}$ values at high and low redshifts (white regions in Figure 5). Uncorrectable images had a non single-valued relationship (green regions). NEI images had undetermined relationships due to a lack of data ($N < 5$) in their corresponding sub-bins (purple regions).

| | N | % |
|---|---|---|
| Correctable | 2,057 | 52% |
| Uncorrectable | 1,732 | 44% |
| NEI | 170 | 4% |
| Total | 3,959 | 100% |

- justify $N > 5$ and spread $< 0.2$ (or find a better way to choose criteria)
- check out corrections for correctable and NEI, show some sample images of corrected galaxies
- show some data for $p_{\mathrm{bar}}$, determine or justify why we won't debiase them

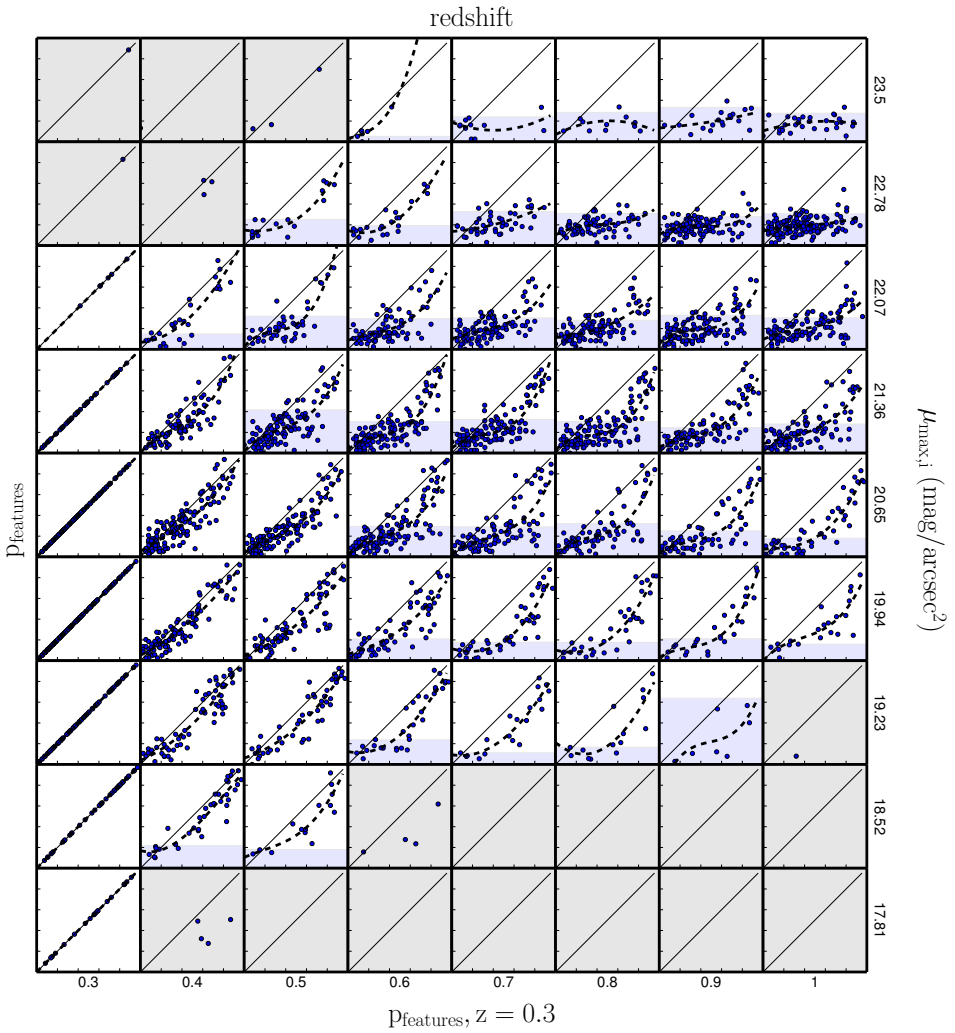


**Figure 5.** Effects of redshift bias in 3,959 images in the FERENGI sample. Each point in a given redshift and surface brightness bin represents a unique galaxy. On the y-axis in each bin is the $p_{features}$ value of the image of that galaxy redshifted to the value corresponding to that redshift bin. On the x-axis is the $p_{features}$ value of the image of the same galaxy redshifted to $z = 0.3$. Regions in which there is a nearly one-to-one relationship between $p_{features}$ at high redshift and $z = 0.3$ are white; those in which there is not are green, and those with not enough data ($N < 5$) are purple.

**Table 5.** Breakdown of what we can correct out of the Hubble data, by sample.

| | AEGIS | COSMOS | GEMS | GOODS-N | GOODS-S | GOODS FULL | SDSS | Total |
|---|---|---|---|---|---|---|---|---|
| Correctable | 1,628 | 15,120 | 1,811 | 739 | 502 | 1,850 | 0 | 21,650 |
| Uncorrectable | 1,869 | 26,184 | 2,407 | 524 | 1,115 | 2,670 | 0 | 34,769 |
| No Correction Needed ($z \leq 0.3$) | 944 | 11,781 | 1,193 | 258 | 258 | 1,083 | 37,545 | 53,062 |
| NEI | 2,753 | 34,432 | 2,271 | 861 | 2,547 | 4,766 | 0 | 47,630 |
| No Redshift Information | 1,313 | 5,291 | 1,622 | 169 | 491 | 788 | 14,316 | 23,990 |
| Total | 8,507 | 92,808 | 9,304 | 2,551 | 4,913 | 11,157 | 51,861 | 181,101 |

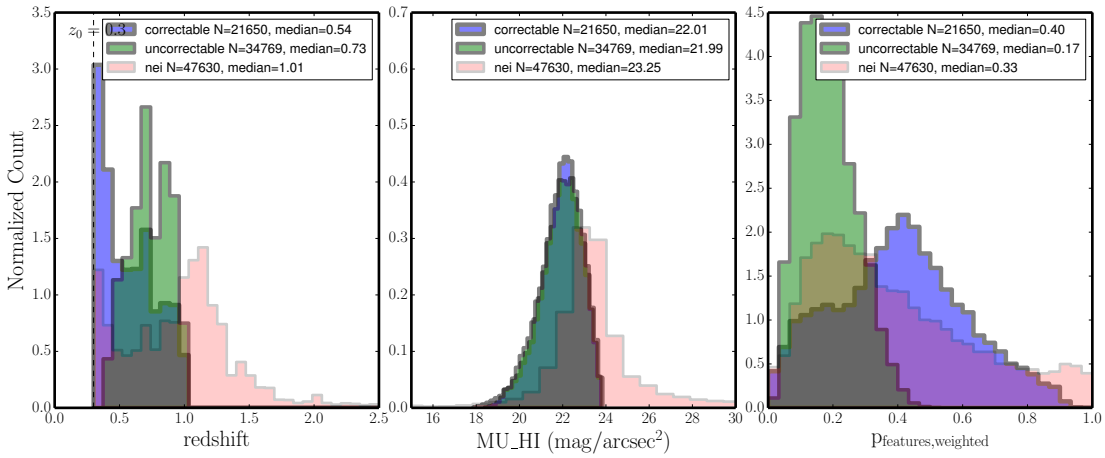


**Figure 6.** Distributions of redshift, surface brightness, and $p_{features}$ for correctable (purple), uncorrectable (green), and NEI (pink) galaxies in the full Hubble sample. The uncorrectable galaxies tend towards higher redshift, slightly lower in surface brightness, and lower values of $p_{features}$ than the correctable galaxies. The long tail of NEI galaxies in redshift and surface brightness demonstrates the limits of the FERENGI sample, for which there is no data at $z > 1$ or $\mu > 24$.

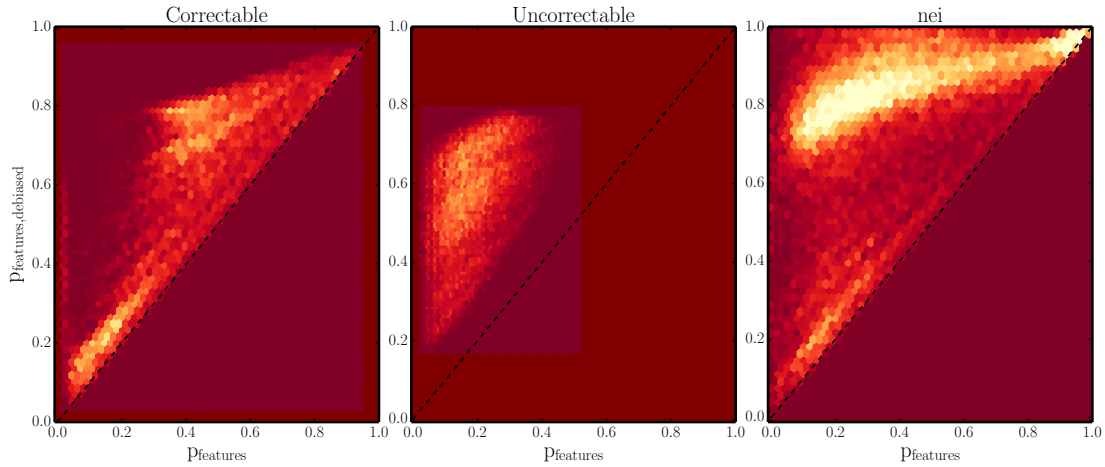


**Figure 7.** Debiased $p_{features}$ corrected to $z = 0.3$ vs weighted $p_{features}$ for the correctable (left), uncorrectable (middle), and NEI (right) galaxies in the Hubble sample.

### 3.4 Results of FERENGI Analysis

We show here the **preliminary** results of citizen scientist classifications of images of galaxies placed at artificial redshifts. Figure 8 shows the **preliminary** range of change of vote fractions for the change of $p_{\rm features}$ with redshift, for galaxies with different vote fraction levels, three ranges of surface-brightness levels and 7 evolutionary corrections (this last bit is indicated by the colour).

#### *3.4.1 TODO LIST*

We need to do:

- Calculate the magnitudes, surface brightnesses and sizes of the galaxies in the FERENGI images....
- Plot of magnitude distribution of galaxies in each of the four GZH subsamples with the magnitudes of our fake galaxies over plotted.
- Instructions of how to link the $z = 0$ $p_X$ values for galaxies with a given size, magnitude (surface brightness) in the GZH images.

### 3.5 Duplicate images

### 3.6 SDSS images

## 4 SUMMARY

Now people go and do science with these awesome Galaxy Zoo Hubble classifications.

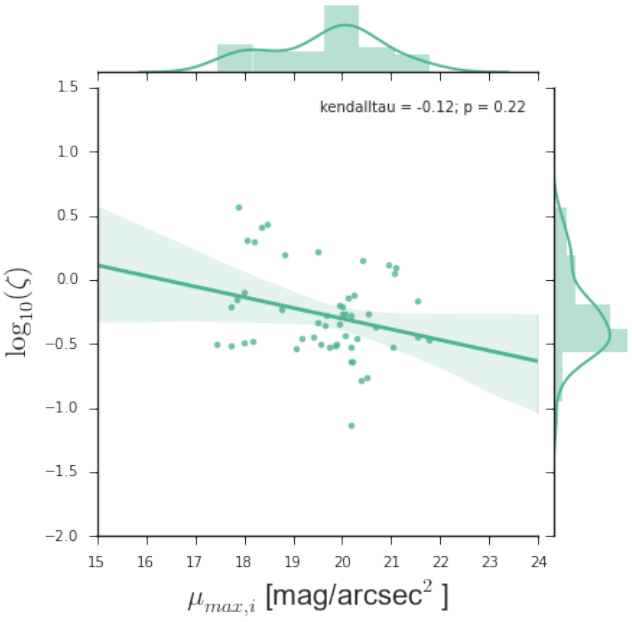


**Figure 3.** All fits for the vote fraction dropoff parameter $\zeta$ for $f_{\rm features}$ in the FERENGI galaxies as a function of surface brightness. This includes only the 51 galaxies with a reasonably bounded range on the dropoff ($-10 < \log(\zeta) < 10$) and sufficient points to fit the function.

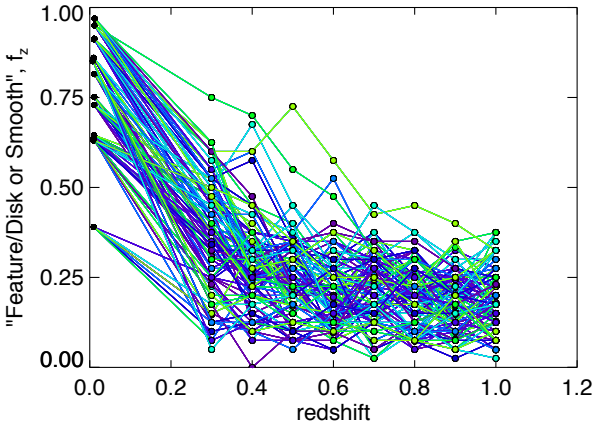


**Figure 8.** Preliminary results of the FERENGI redshifting exercise. WARNING NO USER WEIGHTING.... For a range of vote fraction levels with three surface-brightness levels and 7 evolutionary corrections each (the colours indicate evolutionary correction value with green being $e = 0$, we show the range of evolution of the vote fractions for featured vs. smooth with redshift.

**ACKNOWLEDGEMENTS.** This publication has been made possible by the participation of more than 200,000 volunteers in the Galaxy Zoo project. Their contributions are individually acknowledged at `http://www.galaxyzoo.org/volunteers`. Galaxy Zoo 2 was developed with the help of a grant from The Leverhulme Trust.

We thank ASIAA for hosting the "Citizen Science in Astronomy" workshop, Mar 3-7 2014 in Taipei, Taiwan, at which some of this analysis was done.

HST acknowledgements.

Funding for the SDSS and SDSS-II has been provided by the Alfred P. Sloan Foundation, the Participating Institutions, the National Science Foundation, the U.S. Department of Energy, the National Aeronautics and Space Administration, the Japanese Monbukagakusho, the Max Planck Society, and the Higher Education Funding Council for England. The SDSS Web Site is http://www.sdss.org/.

The SDSS is managed by the Astrophysical Research Consortium for the Participating Institutions. The Participating Institutions are the American Museum of Natural History, Astrophysical Institute Potsdam, University of Basel, University of Cambridge, Case Western Reserve University, University of Chicago, Drexel University, Fermilab, the Institute for Advanced Study, the Japan Participation Group, Johns Hopkins University, the Joint Institute for Nuclear Astrophysics, the Kavli Institute for Particle Astrophysics and Cosmology, the Korean Scientist Group, the Chinese Academy of Sciences (LAMOST), Los Alamos National Laboratory, the Max-Planck-Institute for Astronomy (MPIA), the Max-Planck-Institute for Astrophysics (MPA), New Mexico State University, Ohio State University, University of Pittsburgh, University of Portsmouth, Princeton University, the United States Naval Observatory and the University of Washington.

## REFERENCES

Bamford S. P. et al., 2009, MNRAS, 393, 1324
Barden M., Jahnke K., Häußler B., 2008, ApJS, 175, 105
Griffith R. L. et al., 2012, ApJS, 200, 9
Johnson L. C. et al., 2015, ApJ, 802, 127
Lintott C. J. et al., 2008, MNRAS, 389, 1179
Strauss M. A. et al., 2002, AJ, 124, 1810
Willett K. W. et al., 2013, MNRAS, 435, 2835
York D. G. et al., 2000, AJ, 120, 1579